ECS Journal of Solid State Science and Technology



# Investigation of Deep States in GaN Metal-Oxide-Semiconductor Interfaces

*ECS Journal of Solid State Science and Technology*, 2026 **15** 055002

# Investigation of Deep States in GaN Metal-Oxide-Semiconductor Interfaces

**Yoshihiro Irokawa,[1,z] Mamoru Usami,[2,z] Jun Uzuhashi,[1] Tadakatsu Ohkubo,[1] Toshihide Nabatame,[1,z] and Yasuo Koide[1,3]**

[1]*National Institute for Materials Science, Tsukuba, Ibaraki 305-0044, Japan*
[2]*ASMS Co., Ltd, Shinagawa, Tokyo 141-0022, Japan*
[3]*Meijo University, Nagoya, Aichi 468-8502, Japan*

We previously reported a powerful method to improve dielectric/GaN interface properties: the dummy $SiO_2$ process [Y. Irokawa et al., ECS J. Solid State Sci. Technol. **13**, 085003 (2024)]. Here, GaN metal-oxide-semiconductor (MOS) interfaces prepared with this process were investigated using a sub-bandgap photo-assisted capacitance–voltage technique. GaN MOS interfaces were previously revealed to have deep states, and the dummy process was expected to reduce the number of deep states through its interface modification process. However, the deep state densities in $Al_2O_3$/GaN MOS interfaces after the dummy process did not substantially change compared with those in devices fabricated without the dummy process. Meanwhile, we recently observed oxygen atoms in positions proximate to nitrogen sites in MOS interface regions, with the GaN crystal maintaining the same structure [J. Uzuhashi et al. ECS J. Solid State Sci. Technol. **14**, 085001 (2025)]. We therefore performed first-principles calculations and found that, under certain circumstances, a pair of oxygen atoms replacing nitrogen atoms in GaN created deep states in the bandgap, with slight displacements, similar to *DX* centers; this substitution could be one of the origins of deep states in GaN MOS interfaces.

 [DOI: 10.1149/2162-8777/ae6689]

Manuscript submitted February 12, 2026; revised manuscript received April 22, 2026. Published May 12, 2026.

Improving energy efficiency in electric systems such as invertors and convertors is an important issue from an energy-saving perspective, and transistors based on wide-bandgap semiconductors contribute to the solution to this problem.[1,2] Gallium nitride (GaN) has a relatively wide bandgap of 3.4 eV and has been used in electronic devices to decrease their energy losses.[3–6] Among GaN electronic devices, normally-on-type devices that utilize an AlGaN/GaN heterostructure were developed as early as the 1990s and have displayed excellent performance.[7] Some electric systems, however, require normally-off-type devices for safety reasons, and such devices incorporating GaN have been developed since the 2000s.[8,9] Though various normally-off-type devices have been reported, the metal-oxide-semiconductor (MOS) structure plays a key role in such devices because it offers advantages such as high input impedance, high switching speed, and a large safe operating area.[10]

The interface state density ($D_{it}$) is one of the most important properties in MOS devices because it reflects the carrier trap density between the oxide and semiconductor.[11] GaN MOS interfaces have been known to have a low $D_{it}$ near the conduction band[12]; however, the $D_{it}$ suddenly increases as the energy approaches the valence band.[13–17] The high $D_{it}$ deep in the bandgap should be reduced to improve the device performance[18]; however, the reason for this high $D_{it}$ remains unclear. We previously found that thin crystalline gallium oxide layers exist at the interface between the oxide and GaN and that the properties of the layers can be modified using a newly developed method referred to as the dummy process.[19] We then confirmed that the dummy process restored the disordered atomic arrangement of oxygen and nitrogen in the crystalline gallium oxide layers at the interface in GaN MOS capacitors to some extent and presumed that the improvement of the interfacial-layer crystallinity resulted in the reduction of the flat-band voltage ($V_{fb}$) shifts after positive-bias stressing (PBS).[20] Therefore, whether the dummy process has a positive effect on the $D_{it}$ deep in the bandgap is an interesting topic for investigation.

In this report, we used a sub-bandgap photo-assisted capacitance–voltage (*C–V*) technique and studied the $D_{it}$ deep in the bandgap of GaN MOS capacitors. As a result, we found that the dummy process did not substantially reduce this $D_{it}$, contrary to our expectations. Meanwhile, we recently observed oxygen atoms in positions proximate to nitrogen sites in MOS interface regions (at depths greater than ~1.0 nm), with the GaN crystal being maintained in the same structure.[20] In addition, an oxygen donor impurity in III–V nitrides has been reported to create deep levels in the bandgap under certain conditions.[21–30] Therefore, the observed oxygen atoms in positions proximate to nitrogen sites in GaN MOS interfaces may be related to the higher $D_{it}$ deep in the bandgap of GaN MOS capacitors. Given this consideration, we conducted first-principles calculations and revealed that a pair of oxygen atoms replacing nitrogen atoms in a GaN crystal created deep states in the bandgap, with these oxygen sites slightly shifted from the original nitrogen positions under certain circumstances, similar to *DX* centers, which have been thoroughly studied, especially in $Al_xGa_{1-x}As$.[31] This pair of oxygen atoms replacing nitrogen atoms in GaN could be one of the origins of the experimentally observed deep states in GaN MOS interfaces.

## Experimental

For sub-bandgap photo-assisted *C–V* measurements, we investigated two types of samples: Pt/$Al_2O_3$/*n*-GaN MOS capacitors fabricated using a standard process and MOS capacitors with the same architecture but fabricated using the dummy process. A schematic of the devices is shown in Fig. 1; the details of the device fabrication and measurement procedures have been described elsewhere.[16] Note that trimethylaluminum (TMA) pre-pulses were not used in the atomic layer deposition (ALD) process and that the following recipe was used: $H_2O$ pulse, Ar purge, TMA pulse, and Ar purge.

The atomic-scale $Al_2O_3$/*n*-GaN MOS interface analyses were performed by cross-sectional high-angle annular dark field (HAADF) aberration-corrected scanning transmission electron microscopy (STEM) and energy-dispersive X-ray spectroscopy (EDS) at an incident-electron-beam voltage of 200 kV using a Spectra Ultra S/TEM (Thermo Fisher Scientific). Notably, attention was paid to the preparation of STEM samples to reduce variations in resolution due to changes in sample thickness during STEM–EDS observations. We systematically investigated methods to control TEM sample thickness

[z]E-mail: IROKAWA.Yoshihiro@nims.go.jp; usami@asms.co.jp; NABATAME.Toshihide@nims.go.jp

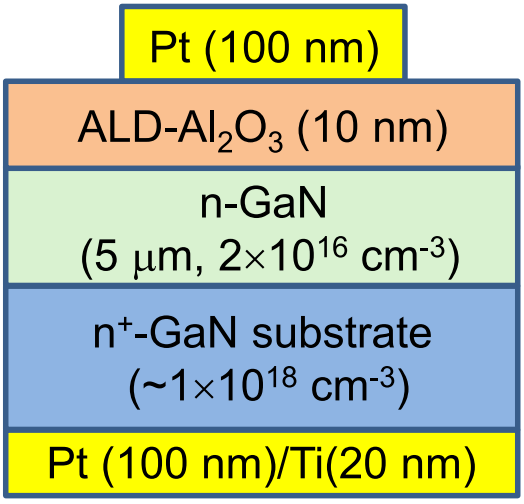


**Figure 1.** Schematic of a Pt/$Al_2O_3$/*n*-GaN MOS capacitor investigated using sub-bandgap photo-assisted *C*–*V* measurements. (ALD = atomic layer deposition).

uniformity using a focused-ion-beam (FIB)–scanning electron microscopy (SEM) dual-beam system, including techniques described in our previous reports,[32,33] and gained a comprehensive understanding of FIB damage to GaN. On the basis of these techniques and insights, we prepared TEM samples with a uniform 30 nm-thickness while minimizing FIB-induced damage.

The first-principles methods are based on density functional theory (DFT) within the generalized gradient approximation (GGA) using the Perdew–Burke–Ernzerhof for solids (PBEsol) exchange-correlation energy functional[34]; the calculations were conducted using the PHASE/0 package based on the projector augmented wave method.[35] The wave functions were expanded in the plane waves up to the kinetic energy cutoff of 340 eV, and all structural models were fully relaxed until the atomic forces were less than $5.1 \times 10^{-3}$ eV Å$^{-1}$. Brillouin zone integrations were carried out using *k*-point meshes of $6 \times 6 \times 4$ for a pure GaN Bravais lattice containing four atoms (two Ga and two N) and $2 \times 2 \times 2$ for supercells. All the calculations were performed with the lattice constants kept at fixed values of $a = 3.20140$ Å and $c = 5.21598$ Å, which were determined by calculation for pure GaN. In addition, all of the calculations in this report were performed without considering spin polarization. Notably, we confirmed that the calculation with spin polarization yielded an electronic state identical to that obtained from the calculation without spin polarization. All of the calculations were performed under a neutral charge condition (without inserting any charge). We used the following configurations as the valence electrons in pseudopotential for gallium, nitrogen, and oxygen: $3d^{10}4s^24p^1$, $2s^22p^3$, and $2s^22p^4$, respectively.

## Results and Discussion

Figures 2a and 2b show the sub-bandgap photo-assisted *C*–*V* characteristics of Pt/$Al_2O_3$/*n*-GaN MOS capacitors fabricated using a standard process and the dummy process, respectively. The incident photon energies are relatively large (2.6, 3.0, and 3.3 eV), and electrons trapped in interfaces at deeper bandgap energies (lower half of the bandgap) were studied. As shown in Fig. 2, after the devices were exposed to light, all of the *C*–*V* curves shifted in the negative voltage direction while almost maintaining their shapes; in addition, larger incident energies led to greater shifts in the initial curves. As discussed elsewhere,[16] these *C*–*V* characteristics reflect donor-type interface trap behavior, where traps act as positive charges after the release of trapped electrons. Notably, to avoid data-analysis difficulties associated with UV light, we used sub-bandgap light in the present study, where the photon energy was less than the bandgap energy of GaN (3.4 eV). Under this condition, holes are not generated. In addition, we speculate that the effects of electron excitation from the valence band to interface traps and/or stepwise excitation of electrons via bulk GaN defect levels (from the valence band) to interface traps are not so significant in our current experiments for the following two reasons: First, if the above-mentioned electron transitions occurred, holes would be generated, possibly resulting in changes in *C*–*V* curve shapes. However, the *C*–*V* curves simply shifted in the negative voltage direction after light irradiation, with their shapes being almost maintained (Fig. 2). Second, the results obtained in our current experiments are consistent with those in previous reports, where the methods differed from ours[13–15]; that is, the $D_{it}$ values near the valence band edge were much higher than those near the conduction band edge at the $Al_2O_3$/GaN interface. Incidentally, the $V_{fb}$ values in Fig. 2 saturated within ~20 min of irradiation for each irradiation energy (2.6, 3.0, and 3.3 eV), suggesting that electron transitions with long time constants do not occur in our current experiments. Figures 3a and 3b show the normalized $V_{fb}$ as a function of the incident photon energy for Pt/$Al_2O_3$/*n*-GaN MOS capacitors fabricated using a standard process and the dummy process and the $D_{it}$ distribution calculated on the basis of the data in Fig. 3a, respectively. In Fig. 3a, $V_{fb}$ measured in the dark was set to be zero, and changes with respect to the $V_{fb}$ in the dark are plotted along the ordinate. In Fig. 3b, the average $D_{it}$ values between two neighboring incident photon energies are plotted at the middle points of these two incident photon energies along the abscissa. Notably, three horizontal dotted lines between two neighboring incident photon energies—0 to 2.6 eV, 2.6 to 3.0 eV, and 3.0 to 3.3 eV—represent the energy ranges where each average $D_{it}$ was calculated. The details of the calculation are found elsewhere.[16] As shown in Fig. 3b, the $D_{it}$ values for the samples fabricated using the two processes do not substantially differ; that is, the $D_{it}$ values at bandgap energies deeper than the mid-gap level are on the order of low-to-mid-$10^{12}$ cm$^{-2}$ eV$^{-1}$ and gradually increase as $E_c - E_t$ approaches the valence band energy of 3.4 eV, irrespective of the

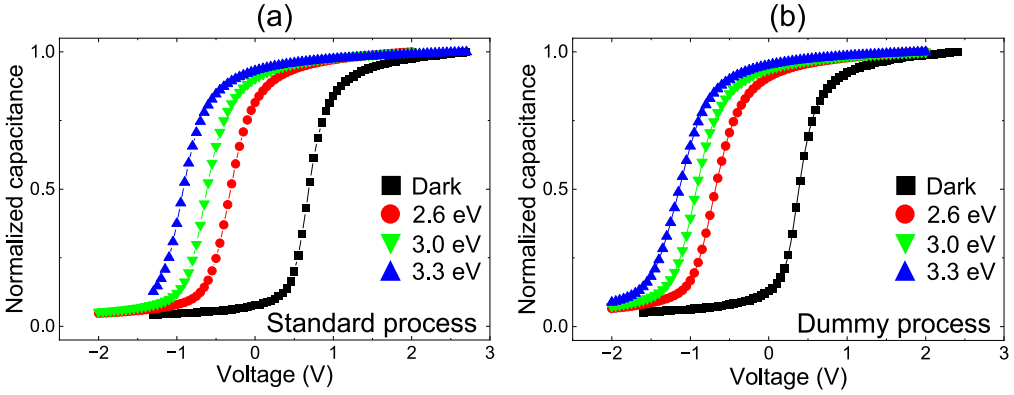


**Figure 2.** Sub-bandgap photo-assisted *C*–*V* characteristics of Pt/$Al_2O_3$/*n*-GaN MOS capacitors fabricated using (a) standard process and (b) dummy process. The incident photon energies are 2.6, 3.0, and 3.3 eV.

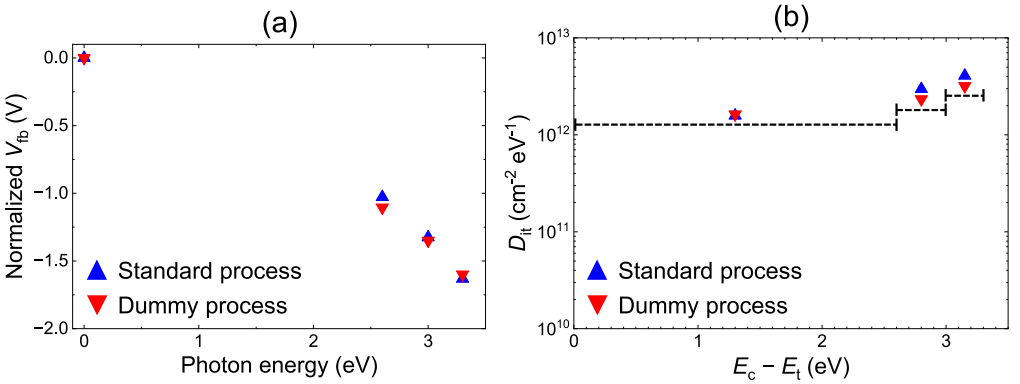


**Figure 3.** (a) Normalized $V_{fb}$ as a function of incident photon energy for Pt/$Al_2O_3$/*n*-GaN MOS capacitors fabricated using a standard and the dummy processes. Here, $V_{fb}$ measured in dark is set to be zero, and changes with respect to the $V_{fb}$ in the dark are plotted along the ordinate. (b) Calculated $D_{it}$ distribution based on the data in (a). The average $D_{it}$ values between two neighboring incident photon energies are plotted at the middle points of these two incident photon energies along the abscissa. Three horizontal dotted lines between two neighboring incident photon energies—0 to 2.6 eV, 2.6 to 3.0 eV, and 3.0 to 3.3 eV—represent the energy ranges where each average $D_{it}$ was calculated.

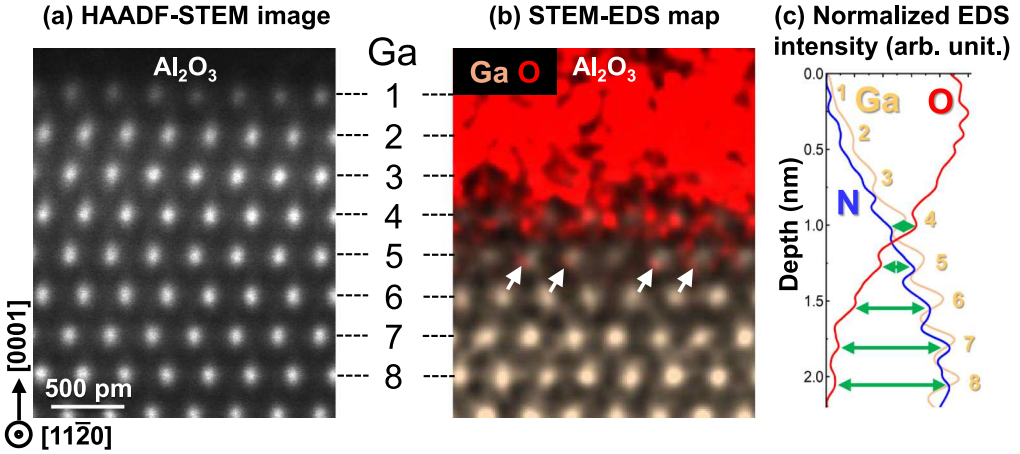


**Figure 4.** (a) HAADF-STEM image. (b) Corresponding EDS element map of gallium and oxygen. Larger spherical areas colored light-orange represent gallium atoms, whereas blurry smaller spherical regions colored red show oxygen atoms. The white arrows indicate the positions where oxygen atoms occupy positions proximate to nitrogen sites in the gallium-polar GaN structure near the $Al_2O_3$/GaN interface. (c) Normalized EDS signal intensity line profile for gallium (light orange), nitrogen (blue), and oxygen (red) for the dummy-processed sample. The first to eighth gallium layers from $Al_2O_3$ are indicated. (Here, the outermost gallium atomic plane observed by HAADF-STEM image is numbered "1".).

fabrication process. We previously confirmed that the dummy process recovered the atomic arrangement of oxygen and nitrogen in the crystalline gallium oxide interfacial layers (at depths less than ~1.0 nm) in GaN MOS structures to some extent, which may be related to the previously reported reduction of the $V_{fb}$ shifts after PBS.[20] Therefore, the dummy process was expected to reduce the $D_{it}$ deep in the bandgap. Contrary to our expectation, however, the dummy process did not substantially reduce the $D_{it}$ at bandgap energies deeper than the mid-gap level. Incidentally, the $D_{it}$ values for samples prepared using the standard and dummy processes were found to be on the order of $10^{11}$ cm$^{-2}$ eV$^{-1}$ at bandgap energies less than 0.6 eV, and these $D_{it}$ values were similar, as we previously reported.[19]

We recently observed oxygen atoms in positions proximate to nitrogen sites in GaN MOS interface regions (at depths greater than ~1.0 nm), with the GaN crystal being maintained in the same structure.[20] Figure 4 shows a HAADF-STEM image (Fig. 4a), the corresponding EDS element map of gallium and oxygen (Fig. 4b), and the normalized EDS signal intensity line profile for gallium, nitrogen, and oxygen (Fig. 4c) for the dummy-processed sample. In Fig. 4, the first to eighth gallium layers from $Al_2O_3$ are indicated. (Here, the outermost gallium atomic plane observed by HAADF-STEM imaging is numbered "1".) In the EDS element map (Fig. 4b), larger spherical areas colored light-orange represent gallium atoms, whereas blurry smaller spherical regions colored red show oxygen atoms. Note that some oxygen atoms occupy positions proximate to nitrogen sites in the gallium-polar GaN structure, as indicated by the white arrows. In addition, according to the normalized EDS signal intensity line profile (Fig. 4c), at depths greater than ~1.0 nm, the oxygen signals and nitrogen signals have peaks at approximately the same depths, as indicated by the green-colored arrows; these results indicate that some of the oxygen atoms might substitute at the nitrogen sites of the GaN crystal structure, with slight displacements, as we reported previously.[20] Note that the EDS data contain an error of a few atomic percent as a technical limitation; the map and profile shown in Figs. 4b and 4c are based on EDS signal intensity to prevent the loss of positional information for the EDS signal as much as possible. To ensure that some of the oxygen atoms occupy positions proximate to nitrogen sites, we conducted observations at multiple locations on several samples.[20,36]

In addition to the above-mentioned atomic-scale interface structural analyses, first-principles calculations have shown that oxygen donor impurities in III–V nitrides create deep levels in the bandgap under certain conditions,[21–25] specifically revealing the following two issues: First, an oxygen donor in GaN did not generally form a deep state. Second, an oxygen donor in $Al_xGa_{1-x}N$ and GaN under pressure did form deep states. (*DX*-like behavior of oxygen in GaN under pressure was also experimentally observed.[26–29]) However,

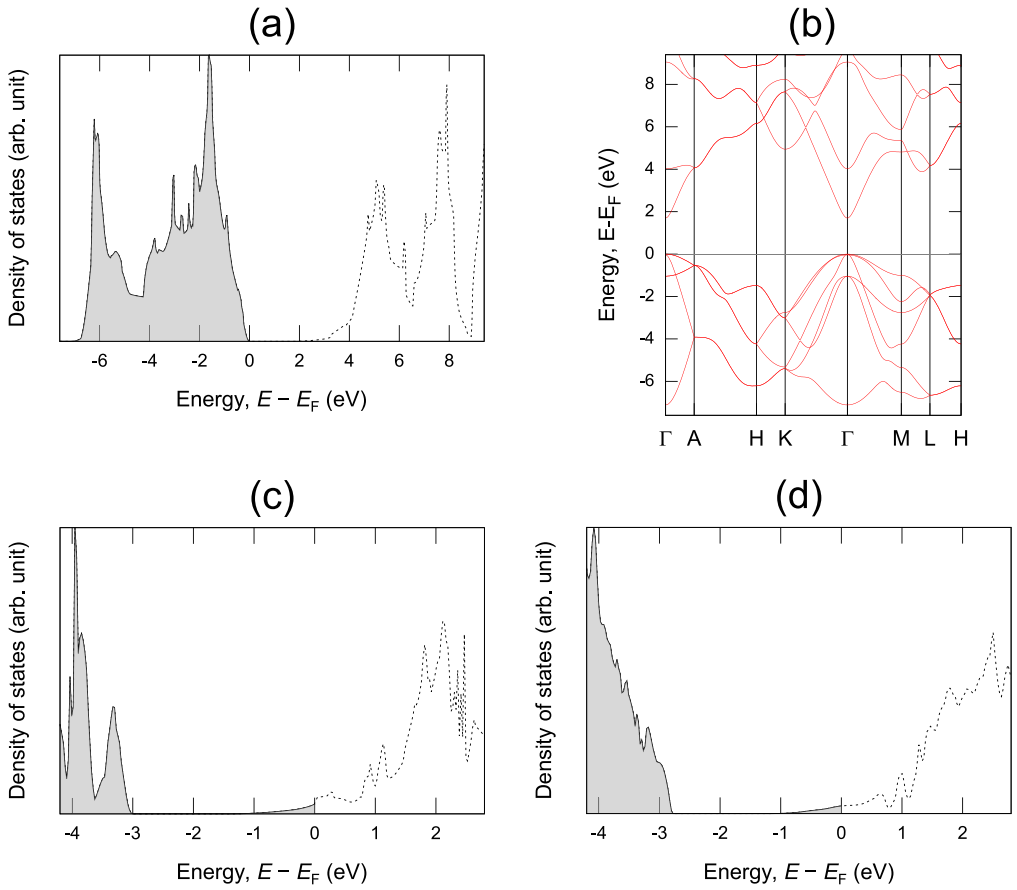


**Figure 5.** (a) Calculated DOS for pure GaN. Here, $E_F$ is defined as the top of the valence band in the presence of a bandgap, and the states are occupied by electrons in gray-colored areas. The conduction band is indicated by dotted lines. (The same labeling convention applies in the following DOS figures in this report.) (b) Calculated energy band structure of pure GaN. (c) Calculated DOS for a 3 × 3 × 2 hexagonal GaN supercell containing 72 atoms, with a single oxygen donor replacing a nitrogen atom in GaN. (d) Calculated DOS for a 2 × 3 × 2 orthorhombic GaN supercell containing 96 atoms, with a single oxygen donor replacing a nitrogen atom in GaN.

these results were reported more than 20 years ago, and recent advances in computers and first-principles calculation methods may enable us to obtain more information regarding oxygen donors in GaN. In addition, the previous research mainly focused on the role of low-concentration oxygen in GaN; the role of high-concentration oxygen, which we have observed, remains unclear. Therefore, the oxygen atoms we observed proximate to nitrogen sites in GaN MOS interface regions (at depths greater than ∼1.0 nm) may be related to the higher $D_{it}$ deep in the bandgap of GaN MOS capacitors even if GaN is not under pressure. On the basis of this consideration, we carried out first-principles calculations.

We first carried out the calculations for pure GaN and GaN supercells with a single oxygen donor replacing a nitrogen atom in GaN to ensure that our calculations worked well. Figures 5a and 5b show the density of states (DOS) and the energy band structure of pure GaN, respectively. In Fig. 5, the Fermi energy ($E_F$) is defined as the top of the valence band in the presence of a bandgap; the states in gray areas are occupied by electrons. In addition, the conduction band is represented by dotted lines. (The same labeling scheme is used in subsequent DOS figures in this report.) The data shown in Figs. 5a and 5b indicate that GaN has a direct bandgap of ∼1.7 eV, which is smaller than the actual bandgap of GaN (3.4 eV). Notably, DFT within the GGA typically underestimates bandgap values,[37] and we do not discuss the calculated bandgap values in this report. We also obtained the optimized lattice constants for GaN ($a = 3.20140$ Å and $c = 5.21598$ Å), which are close to the experimentally obtained values (e.g., $a = 3.18926$ Å and $c = 5.18523$ Å for bulk GaN fabricated by hydride vapor phase epitaxy).[38] Figures 5c and 5d show the DOS for a 3 × 3 × 2 hexagonal GaN supercell and a 2 × 3 × 2 orthorhombic GaN supercell containing 72 and 96 atoms, respectively, with a single oxygen donor replacing a nitrogen atom in GaN. As shown in both figures, the conduction bands have tail states below 0 eV that are filled with electrons, which means that a single oxygen donor replacing a nitrogen atom in GaN creates shallow states, consistent with previous reports.[39,40]

We next replaced two nitrogen atoms in a 3 × 3 × 2 hexagonal GaN supercell containing 72 atoms, corresponding to a ∼2.8% oxygen concentration in GaN. The positions of the replaced nitrogen atoms correspond to those of two nitrogen atoms in a four-atom primitive cell of GaN and are located in two adjacent nitrogen planes perpendicular to the [0001] direction. Note that no previous studies have considered the substitution of two oxygen atoms into GaN. Figures 6a–6c show the atomic arrangements after the structural optimization was performed. Here, Figs. 6b and 6c show magnified images of the upper and lower oxygen atoms in Fig. 6a, respectively, and Fig. 6d shows the DOS for the supercell. As shown in Fig. 6d, deep levels are formed in this particular case. Figures 6a–6c show that the two oxygen atoms are in different positions from those occupied by the original nitrogen atoms; that is, both of the oxygen atoms move far away from each other, breaking their gallium–oxygen bonds, which are shown by dotted lines in Figs. 6b and 6c. Notably, a large displacement of a donor atom was previously reported as one of the characteristics of *DX* centers[21]; therefore, the oxygen-atom behavior observed in Figs. 6a–6c is similar to that of *DX* centers. Our results show that two oxygen donors create deep states without pressure on GaN, unlike the results of previous studies, which considered substitution by only one oxygen donor.[21–24] Figure 7 shows contour plots of the charge

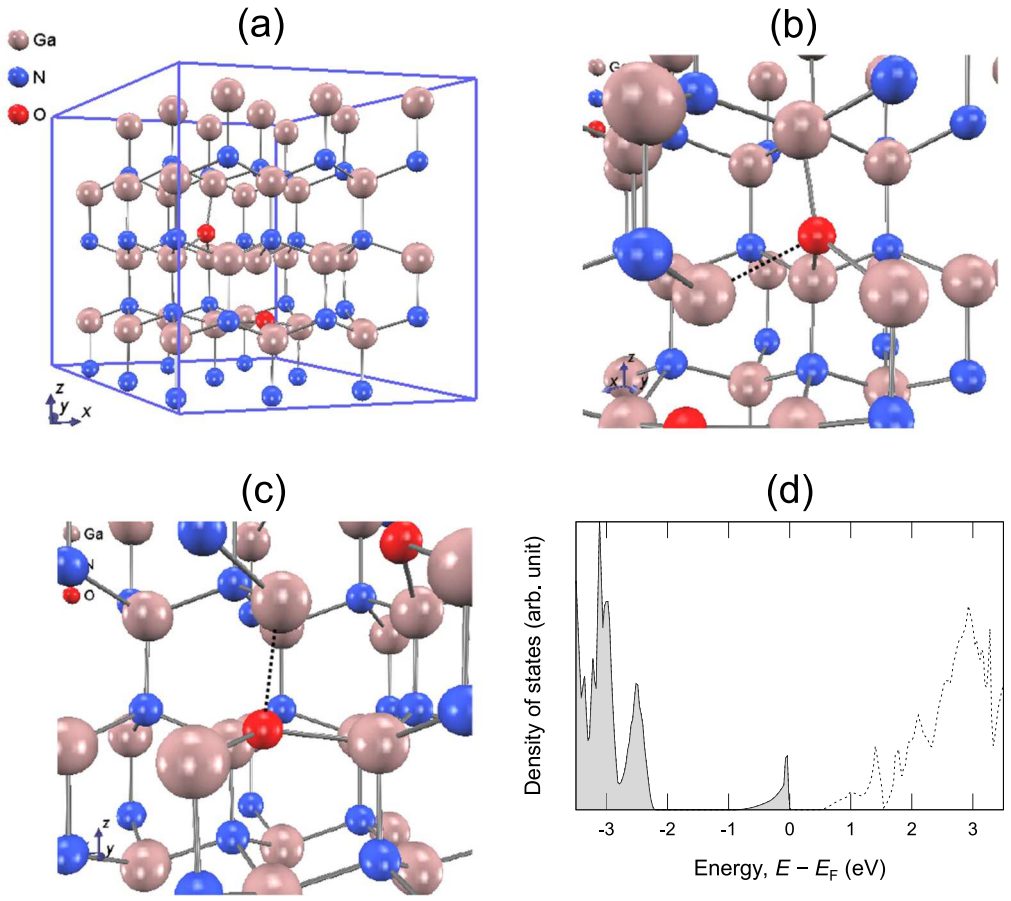


**Figure 6.** (a) 3 × 3 × 2 hexagonal GaN supercell after the structural optimization; the supercell contains 72 atoms with two nitrogen atoms replaced with oxygen, corresponding to a ∼2.8% oxygen concentration in GaN. The positions of the replaced nitrogen atoms correspond to those of two nitrogen atoms in a four-atom primitive cell of GaN and are located in two adjacent nitrogen planes perpendicular to the [0001] direction. (b) Magnified image of the upper oxygen atom in (a). The broken gallium–oxygen bond is shown as a dotted line. (c) Magnified image of the lower oxygen atom in (a). The broken gallium–oxygen bond is shown as a dotted line. (d) Calculated DOS for the supercell shown in (a).

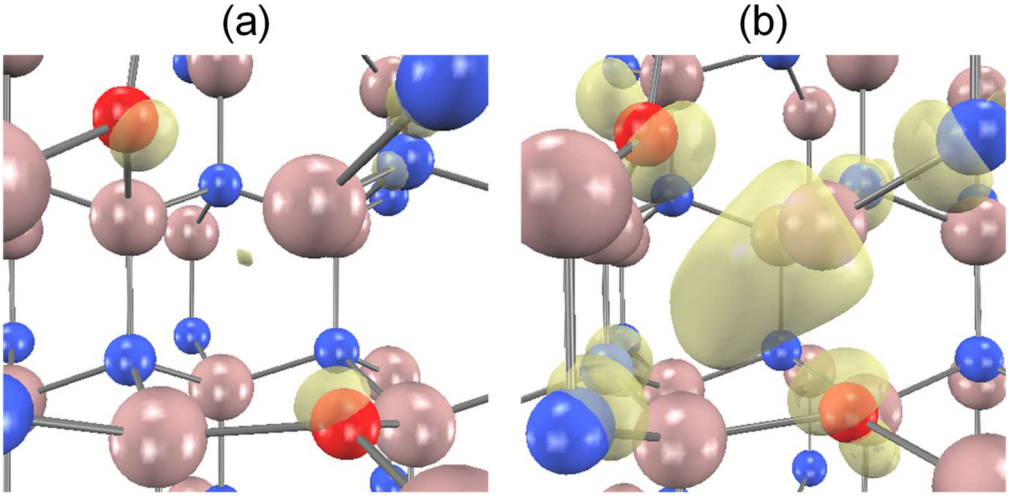


**Figure 7.** Contour plots of the charge density in deep states (energy range from −1 to 0 eV in Fig. 6d) around two oxygen atoms, as shown in Fig. 6a; isosurface values of 0.025 e/Bohr$^3$ (a) and 0.005 e/Bohr$^3$ (b) are displayed.

density in deep states (energy range from −1 to 0 eV in Fig. 6d) around two oxygen atoms (Fig. 6a); isosurface values of 0.025 and 0.005 e/Bohr$^3$ are displayed in Figs. 7a and 7b, respectively. As shown in Fig. 7, the electron density around the two oxygen atoms is high and the trapped charges amount to approximately two electrons. Note that this calculation was performed under a neutral charge condition (i.e., without the insertion of any charge), unlike the calculations in previous reports[21–24]; that is, in the previous reports, the deep donor formation process was described by the following reaction[21]:

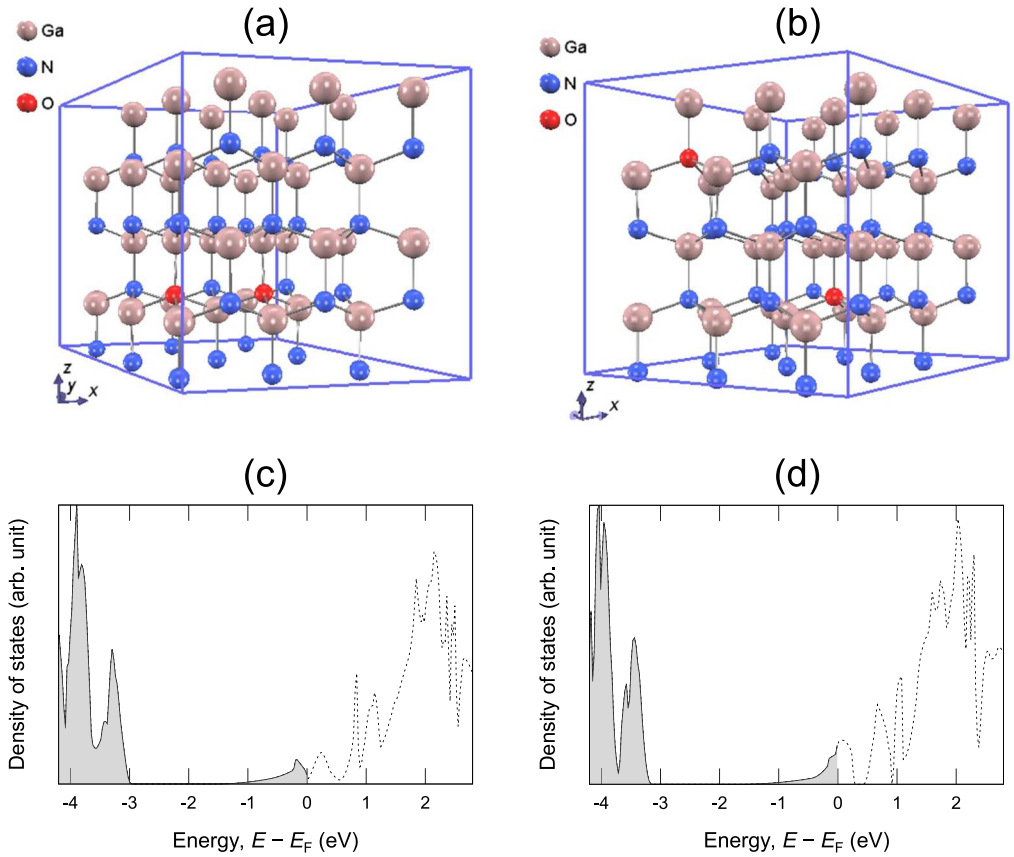


**Figure 8.** (a) 3 × 3 × 2 hexagonal GaN supercell after the structural optimization, containing 72 atoms with two nitrogen atoms replaced with oxygen, corresponding to a ∼2.8% oxygen concentration in GaN. The replaced nitrogen atoms are located in the closest position in the same crystal plane perpendicular to the [0001] direction. (b) 3 × 3 × 2 hexagonal GaN supercell after the structural optimization, containing 72 atoms with two nitrogen atoms replaced with oxygen atoms, corresponding to a ∼2.8% oxygen concentration in GaN. The replaced nitrogen atoms are located in the farthest positions from each other, considering periodic boundary conditions. (c) Calculated DOS for the supercell shown in (a). (d) Calculated DOS for the supercell shown in (b).

$$2d^0 \rightarrow DX^- + d^+, \qquad [1]$$

where $d$ is a substitutional shallow impurity, $DX$ represents a broken-bond (BB) state, and the superscripts specify the charge states. As shown in Eq. 1, the $DX$ is assumed to acquire electrons from the other impurity.

Meanwhile, we investigated how the arrangement of the two oxygen atoms in the same 3 × 3 × 2 hexagonal GaN supercell containing 72 atoms affects the DOS and the stability. First, we replaced two nitrogen atoms located in the closest position in the same crystal plane perpendicular to the [0001] direction; Figs. 8a and 8c show the atomic arrangement after the structural optimization and the DOS for the supercell, respectively. As shown in Fig. 8a, the two inserted oxygen atoms occupy similar positions to the original nitrogen atoms after the structural optimization, unlike those in Fig. 6a; in addition, as shown in Fig. 8c, the conduction band has tail states below 0 eV that are filled with electrons, creating shallow states, as in the case of single-oxygen-atom insertion (Fig. 5c and 5d). Second, we replaced two nitrogen atoms located at the farthest positions from each other, considering periodic boundary conditions; Figs. 8b and 8d show the atomic arrangement after the structural optimization and the DOS for the supercell, respectively. As shown in Figs. 8b and 8d, the two inserted oxygen atoms occupy similar locations to the original nitrogen atoms and deep states are not formed, as in the case shown in Fig. 8a and 8c. With respect to the total energy, the atomic arrangement shown in Fig. 6a exhibits the lowest, whereas those shown in Figs. 8a and 8b are 73.5 and 106 meV higher, respectively, than that shown in Fig. 6a. In brief, the results obtained from Figs. 6–8 show that the atomic arrangement in Fig. 6 is the most stable and that two oxygen atoms replacing nitrogen atoms in an arrangement shown in Fig. 6 create deep states in the bandgap. These deep states trap electrons, where the distorted lattice stemming from the oxygen displacements is likely stabilized by the trapped charges and appears to result in the formation of these deep states. These deep states shown in Fig. 6d could be one of the origins of the large $D_{it}$ at bandgap energies deeper than the mid-gap level (Fig. 3b). Note that, in the 72-atom system, we confirmed that no energy barrier exists for the transformation between a shallow state and a deep state. Incidentally, another example of a stabilized pair of dopant atoms in close proximity can be seen in diamond.[41]

We subsequently investigated the effects of the oxygen concentration in GaN. First, we replaced two nitrogen atoms in a 2 × 3 × 2 orthorhombic GaN supercell containing 96 atoms, corresponding to a ∼2.1% oxygen concentration in GaN. This oxygen concentration is lower than that in the previously discussed model (∼2.8%). The atomic arrangements in Figs. 9a and 9b correspond to those in Figs. 6a and 8a, respectively, and the DOS corresponding to Figs. 9a and 9b is shown in Figs. 9c and 9d, respectively. As shown in Figs. 9a and 9c, the two inserted oxygen atoms are displaced, similar to those in Fig. 6a, and deep states are formed. However, as shown in Fig. 9b and 9d, the two inserted oxygen atoms occupy similar sites to the original nitrogen atoms, and deep states are not formed, as in the case in Figs. 8a and 8c. With respect to the total energy, the atomic arrangement in Figs. 9b is 53.2 meV lower than that in Fig. 9a, whereas the atomic arrangement in Fig. 9a is locally stable. Second, we replaced two nitrogen atoms in a 4 × 4 × 3 hexagonal GaN supercell containing 192 atoms, corresponding to a ∼1.0% oxygen concentration in GaN. Notably, the oxygen concentration is even lower. The atomic arrangements in Figs. 10a and 10b correspond to

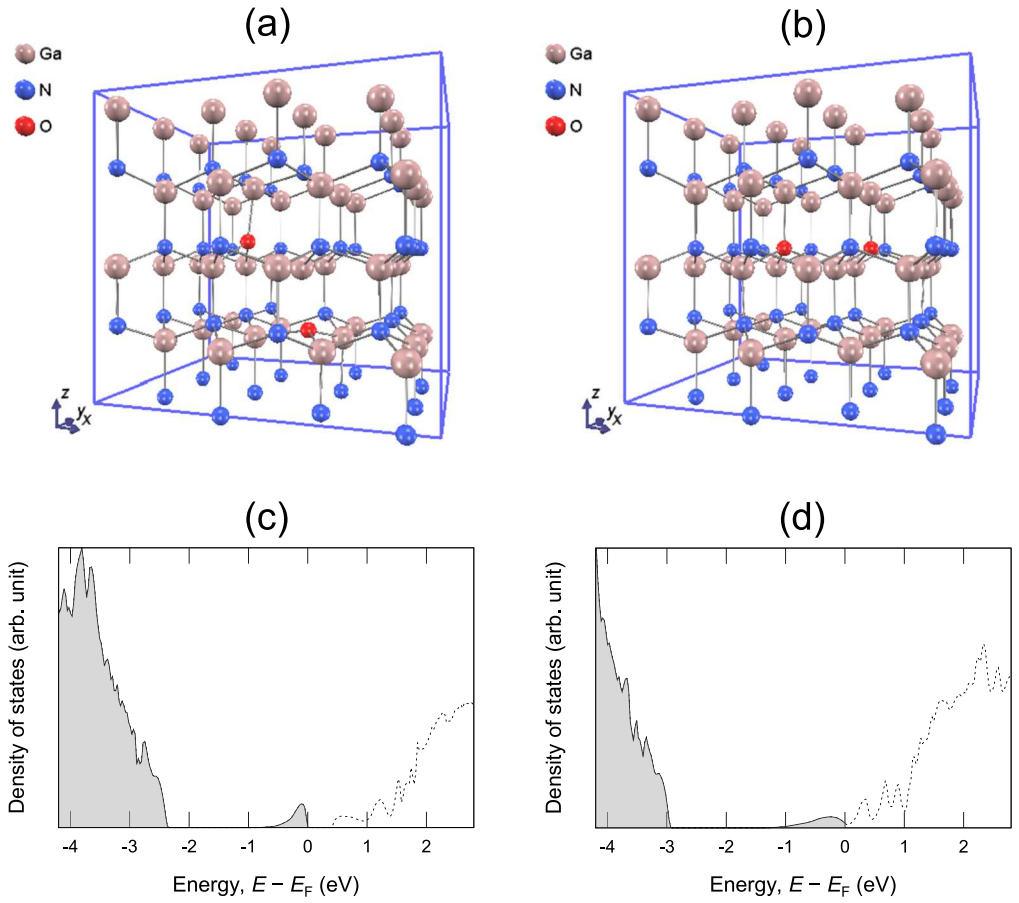


**Figure 9.** (a) 2 × 3 × 2 orthorhombic GaN supercell containing 96 atoms, corresponding to a ∼2.1% oxygen concentration in GaN. The atomic arrangement corresponds to that in Fig. 6a. (b) 2 × 3 × 2 orthorhombic GaN supercell containing 96 atoms, corresponding to a ∼2.1% oxygen concentration in GaN. The atomic arrangement corresponds to that in Fig. 8a. (c) Calculated DOS for the supercell shown in (a). (d) Calculated DOS for the supercell shown in (b).

those in Figs. 6a and 8b, respectively, and the DOS in Figs. 10a and 10b is shown in Figs. 10c and 10d, respectively. Figure 10c shows that deep states are no longer formed, even for the same atomic arrangement as in Figs. 6a and 9a where the deep states are actually formed. In addition, the total energy for the atomic arrangement in Fig. 10a is 68.6 meV higher than that for the arrangement in Fig. 10b. In summary, the results obtained from Figs. 9 and 10 are that two oxygen atoms replacing nitrogen atoms do not create deep states (with a stable energy) in any arrangement when the oxygen concentration is low.

At this point, we are uncertain whether the oxygen-induced deep states studied here are identical to *DX* centers formerly investigated in $Al_xGa_{1-x}As$ in the following three aspects: First, an energy barrier for the transformation between a shallow state and a deep state, which is an important characteristic feature of the *DX* center,[42] does not exist in our 72-atom system calculations. (Two inserted oxygen atoms are displaced from the original nitrogen atom positions with no energy barrier, resulting in the atomic arrangement shown in Fig. 6a). Second, the displacements of the oxygen atoms appear to be relatively small in our calculations (e.g., the upper oxygen atom does not move beyond the plane formed by three gallium atoms bonding to the oxygen (Fig. 6b), unlike an α-broken-bond-type *DX* center described in a previous report[21]). Third, the charge states of the two inserted donors differ, as previously mentioned. Furthermore, the oxygen concentration in GaN clearly plays a critical role in the formation of oxygen-induced deep states. Notably, the relationship between the oxygen concentration in GaN and the formation of deep states was suggested in previous reports[25,30]; however, the details are unclear even now. A similar phenomenon in which the formation of donor-induced deep states depends on the donor concentration was reported in a study of Si-doped GaAs based on experimental results.[43] Our current understanding of why deep state formation strongly depends on the oxygen concentration is as follows: To form deep states, a certain amount of oxygen displacement in an energetically stabilized state is critical, as previously reported[21]; some negative charges are required to stabilize such oxygen displacements. We speculate that the position and concentration of introduced oxygen atoms would be strongly related to the above-mentioned issues.

Throughout this report, we have investigated deep states in GaN MOS interfaces both experimentally and theoretically and have revealed that a pair of oxygen atoms replacing nitrogen atoms in GaN creates deep states in the bandgap, with slight displacements under certain circumstances. However, the created deep states exist only in the middle of the bandgap (Fig. 6d) and do not explain the experimentally observed $D_{it}$ distribution shown in Fig. 3b, where the density of electron traps near the valence band is even higher than that in the middle of the bandgap. To consider this issue, we inspected our calculation model. On the basis of our previous research,[20] the $Al_2O_3$/GaN interface consists of $Al_2O_3$, a highly oriented crystalline $GaO_xN_y$ interfacial layer, and pure GaN (here, Si-doped GaN), as shown in Fig. 11. The $GaO_xN_y$ layer exhibits a graded composition; that is, the oxygen content $x$ decreases toward the bulk GaN region, whereas the nitrogen content $y$ increases toward the bulk GaN region. In addition, the gallium atoms occupy the same positions as those in bulk GaN, whereas some oxygen and nitrogen atoms are in irregular positions near the $Al_2O_3$ (at depths shallower than ∼1.0 nm). However, at depths greater than ∼1.0 nm, the $GaO_xN_y$ interfacial layer has a similar crystal structure to bulk GaN, with oxygen atoms in positions proximate to nitrogen sites. The $GaO_xN_y$ interface layer is formed in GaN as a result of oxygen diffusion. An EDS signal associated with this diffused oxygen can be

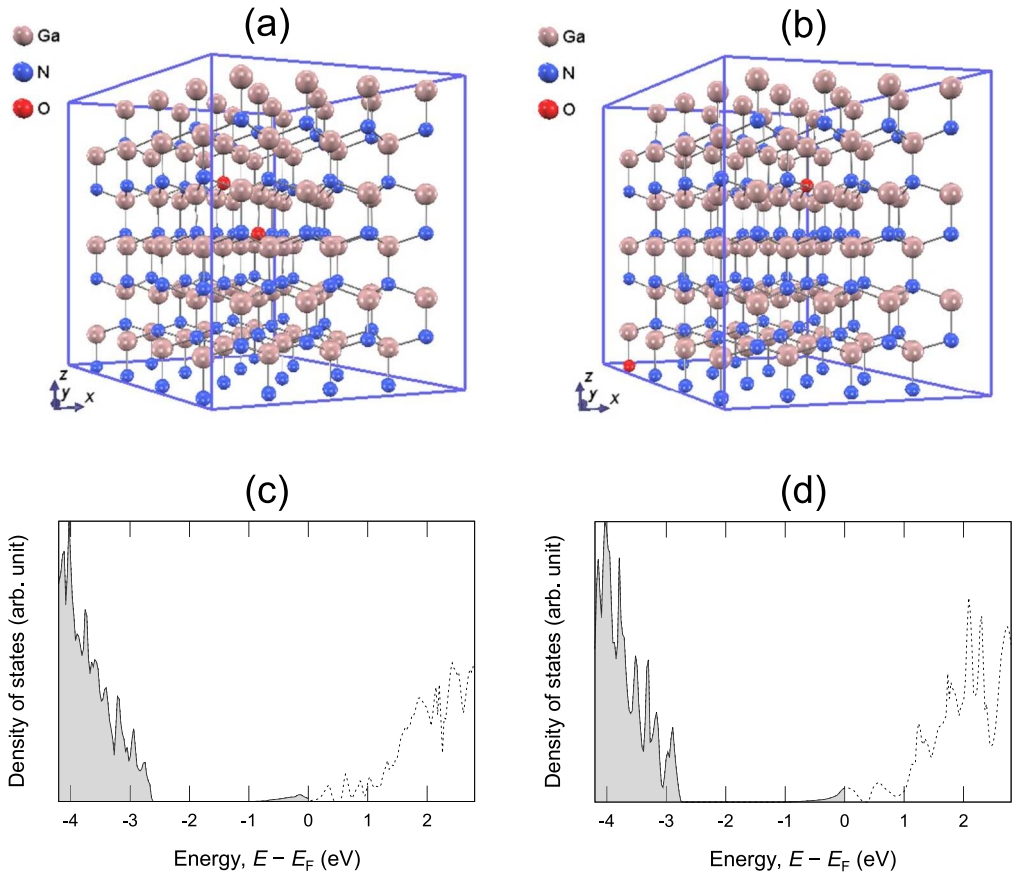


**Figure 10.** (a) 4 × 4 × 3 hexagonal GaN supercell containing 192 atoms, corresponding to ∼1.0% oxygen concentration in GaN. The atomic arrangement corresponds to that in Fig. 6a. (b) 4 × 4 × 3 hexagonal GaN supercell containing 192 atoms, corresponding to a ∼1.0% oxygen concentration in GaN. The atomic arrangement corresponds to that in Fig. 8b. (c) Calculated DOS for the supercell shown in (a). (d) Calculated DOS for the supercell shown in (b).

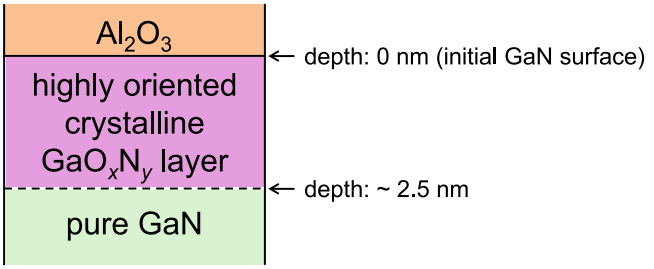


**Figure 11.** Schematic of the $Al_2O_3$/GaN interface.

detected to a depth of ∼2.5 nm.[20] Given the detection limit of EDS (a few atomic percent), oxygen could diffuse into the GaN more deeply at dopant-level concentrations. Since the $GaO_xN_y$ layer is compositionally graded and has a high degree of crystallinity, its composition and crystal structure continuously change in the depth direction towards those of bulk crystalline GaN. We therefore speculate that its interface with GaN has a low defect density. In our calculations, the oxygen concentration is a few atomic percent, with two oxygen atoms replacing two nitrogen atoms in a perfect GaN crystal; these circumstances approximately reflect those in less defective deeper regions of the $GaO_xN_y$ layer (at a depth of ∼2.5 nm in Fig. 11). In addition, we speculate that the $Al_2O_3/GaO_xN_y$ interface also has a low defect density because gallium atoms in the $GaO_xN_y$ layer occupy the same positions as those in bulk GaN. We therefore believe that the proposed model, which considers only defects in the $GaO_xN_y$ layer, is realistic for GaN MOS systems, because both the $Al_2O_3/GaO_xN_y$ and $GaO_xN_y$/GaN interfaces are considered to have a low defect density. Moreover, in the case of $SiO_2$/GaN MOS interfaces, we observed oxygen diffusion into GaN,[18] which possibly even occurred unintentionally by natural oxidation.[18,36] We therefore consider that diffusion of oxygen is a universal phenomenon for GaN surfaces and interfaces and that our defect formation mechanism is applicable to any GaN MOS system. Based on previous studies on deep states created by oxygen donors in GaN,[21–25] we initially substituted two oxygen atoms at nitrogen positions in the present study. In the present study, calculation conditions such as the degree of crystallinity and the oxygen concentration were chosen to represent those at a depth of ∼2.5 nm in Fig. 11. However, in the $GaO_xN_y$ interface layer, the oxygen concentration increases with decreasing distance from the $Al_2O_3$. For example, the oxygen concentration is ∼40% at a depth of 1.0 nm,[20] which is much higher than that in our current calculations. In addition, we also observed that oxygen atoms were in irregular positions in shallower parts of the $GaO_xN_y$ layer, even in samples prepared with the dummy process.[20] As explained earlier, oxygen displacement is closely related to the deep states; irregular positions such as interstitial sites can be regarded as having much larger displacements of oxygen atoms from nitrogen sites than that obtained in the present study. Therefore, we consider that calculations involving oxygen positions and concentrations might result in the observation of deeper states in the bandgap. Such calculations would reflect more defective shallower regions of the $GaO_xN_y$ interfacial layer, unlike our present study considering less defective deeper regions of the interfacial layer. In addition, nitrogen atoms in irregular sites might also create deep states, which we did not consider in the present study. Given this perspective, the reason for the higher $D_{it}$ deep in the bandgap of GaN MOS capacitors (Fig. 3b) can be speculated to be as follows: as mentioned above, we previously confirmed that the dummy process improved the crystallinity of the $GaO_xN_y$ interfacial layer to some

extent,[20] which may be reflected in the slightly lower $D_{it}$ values near the valence band for the sample produced using the dummy process (Fig. 3b). However, recovery of the crystallinity was incomplete; some oxygen and nitrogen atoms were left in irregular sites, which might be related to the large $D_{it}$ at bandgap energies deeper than the mid-gap level. We are also aware that our model is an approximation and does not reflect the $Al_2O_3$/GaN interface correctly, which could also be the reason why the calculated deep states exist only in the middle of the bandgap. In summary, to resolve the contradiction between the experimentally obtained deep-state distribution and the calculated deep states, more extensive calculations that take into account different oxygen and nitrogen positions, with more than two oxygen atoms introduced, and/or using hybrid functionals would be necessary in future studies.

## Conclusions

We used a sub-bandgap photo-assisted *C–V* technique and studied the $D_{it}$ deep in the bandgap of GaN MOS capacitors. As a result, we found that the dummy process did not substantially reduce this $D_{it}$ value, contrary to our expectations. However, we directly observed that some oxygen atoms occupy positions proximate to nitrogen sites near the $Al_2O_3$/GaN interface. In addition, our first-principles calculations revealed that, under certain circumstances, a pair of oxygen atoms replacing nitrogen atoms in GaN created deep states in the bandgap, with these oxygen sites being slightly shifted from the original nitrogen positions, similar to *DX* centers. These oxygen-induced deep states might be one of the origins of the observed higher $D_{it}$ at deeper bandgap energies in GaN MOS capacitors. The elucidation of the deep-state formation mechanism is an important subject for future studies, and more detailed calculations will be necessary to explain the experimentally observed $D_{it}$ distribution more correctly; that is, the present calculations only considered less defective deeper regions of the highly crystalline $GaO_xN_y$ interfacial layer. Therefore, calculations corresponding to more defective shallower regions of the interfacial layer could resolve the contradiction between the experimentally obtained deep state distribution and the calculated deep states.

Finally, in this report, we introduce the possibility that GaN itself could be the origin of the deep states in GaN MOS interfaces by incorporating oxygen. The incorporated oxygen could change the GaN surface/interface properties; in fact, surface property changes have been reported for MBE-grown GaN upon exposure to air, where the surface $E_F$ drastically shifted toward the conduction band edge after air exposure.[44–46] In this case, we speculate that some oxygen atoms replace nitrogen atoms, acting as shallow donors, at somewhat deeper regions where the oxygen concentration is low. This could also lead to unintentional realization of buried-channel devices in GaN MOS field-effect transistors, which could be one of the reasons why such devices exhibit relatively high mobility.

## Acknowledgments

This research was supported in part by the Ministry of Education, Culture, Sports, Science and Technology, Japan (NEXT), through its "Creation of Innovative Core Technology for Power Electronics" Program Grant Number JPJ009777, ARIM (JPMXP1223NM5088), and JSPS KAKENHI Grant Numbers 23K03949. A part of this work was supported by the Electron Microscopy Unit, National Institute for Materials Science (NIMS). The authors thank Kyoko Suzuki for her technical support with the STEM observations. The authors thank Dr Keisuke Masuda for fruitful discussions.

## ORCID

Yoshihiro Irokawa https://orcid.org/0000-0002-6531-4356
Mamoru Usami https://orcid.org/0009-0002-3188-7380
Jun Uzuhashi https://orcid.org/0000-0003-2023-8158
Tadakatsu Ohkubo https://orcid.org/0000-0003-3548-1951
Toshihide Nabatame https://orcid.org/0000-0002-5973-0230
Yasuo Koide https://orcid.org/0000-0001-8321-9822

## References

1. T. Kachi, *Appl. Phys. Express*, **19**, 010103 (2026).
2. T. Kimoto and J. A. Cooper, *Fundamentals of Silicon Carbide Technology* (Wiley, Singapore) 445 (2014).
3. S. J. Pearton, F. Ren, A. P. Zhang, and K. P. Lee, *Mater. Sci. Eng. R*, **30**, 55 (2000).
4. T. Oka, *Jpn. J. Appl. Phys.*, **58**, SB 0805 (2019).
5. K. Ito, S. Iwasaki, K. Tomita, E. Kano, N. Ikarashi, K. Kataoka, D. Kikuta, and T. Narita, *Appl. Phys. Express*, **16**, 074002 (2023).
6. Y. Ichikawa, K. Ueno, T. Kondo, R. Tanaka, S. Takashima, and J. Suda, *Jpn. J. Appl. Phys.*, **63**, 02SP31 (2024).
7. R. Quay, *Gallium Nitride Electronics* (Springer, Berlin) 71 (2008).
8. S. Jang et al., *J. Electron. Mater.*, **35**, 685 (2006).
9. H. Kambayashi, Y. Niiyama, S. Ootomo, T. Nomura, M. Iwami, Y. Satoh, S. Kato, and S. Yoshida, *IEEE Electron Device Lett.*, **28**, 1077 (2007).
10. B. J. Baliga, *Modern power devices* (Wiley, New York) 263 (1992).
11. T. Kimoto and J. A. Cooper, *Fundamentals of Silicon Carbide Technology* (Wiley, Singapore) 219 (2014).
12. H. C. Casey Jr, G. G. Fountain, R. G. Alley, B. P. Keller, and S. P. DenBaars, *Appl. Phys. Lett.*, **68**, 1850 (1996).
13. C. M. Jackson, A. R. Arehart, E. Cinkilic, B. McSkimming, J. S. Speck, and S. A. Ringel, *J. Appl. Phys.*, **113**, 204505 (2013).
14. R. D. Long et al., *Appl. Phys. Lett.*, **103**, 201607 (2013).
15. X. Liu et al., *Appl. Phys. Lett.*, **119**, 015303 (2016).
16. Y. Irokawa, T. Nabatame, K. Yuge, A. Uedono, A. Ohi, N. Ikeda, and Y. Koide, *AIP Adv.*, **9**, 085319 (2019).
17. T. Kobayashi, K. Tominaga, M. Nozaki, T. Shimura, and H. Watanabe, *Appl. Phys. Express*, **17**, 011003 (2024).
18. Y. Irokawa, K. Mitsuishi, T. Izumi, J. Nishii, T. Nabatame, and Y. Koide, *ECS J. Solid State Sci. Technol.*, **12**, 055007 (2023).
19. Y. Irokawa, T. Nabatame, T. Sawada, M. Miyamoto, H. Miura, K. Tsukagoshi, and Y. Koide, *ECS J. Solid State Sci. Technol.*, **13**, 085003 (2024).
20. J. Uzuhashi, Y. Irokawa, T. Nabatame, T. Ohkubo, and Y. Koide, *ECS J. Solid State Sci. Technol.*, **14**, 085001 (2025).
21. C. H. Park and D. J. Chadi, *Phys. Rev. B*, **55**, 12995 (1997).
22. C. G. Van de Walle, *Phys. Rev. B*, **57**, R2033 (1998).
23. C. G. Van de Walle, C. Stampfl, and J. Neugebauer, *J. Cryst. Growth*, **189/190**, 505 (1998).
24. C. G. Van de Walle, J. Neugebauer, C. Stampfl, M. D. McCluskey, and N. M. Johnson, *Acta Phys. Pol. A*, **96**, 613 (1999).
25. C. Liu and J. Kang, *Opt. Mater.*, **23**, 169 (2003).
26. C. Wetzel, T. Suski, J. W. Ager III, E. R. Weber, E. E. Haller, S. Fischer, B. K. Meyer, R. J. Molnar, and P. Perlin, *Phys. Rev. Lett.*, **78**, 3923 (1997).
27. C. Wetzel, J. W. Ager III, M. Topf, B. K. Meyer, H. Amano, and I. Akasaki, *Physica B*, **273-274**, 109 (1999).
28. C. Wetzel, H. Amano, I. Akasaki, J. W. Ager III, I. Grzegory, M. Topf, and B. K. Meyer, *Phys. Rev. B*, **61**, 8202 (2000).
29. C. Wetzel, H. Amano, I. Akasaki, J. W. Ager III, I. Grzegory, and B. K. Meyer, *Physica B*, **302-303**, 23 (2001).
30. T. W. Kang, C. S. Park, and T. W. Kim, *Appl. Surf. Sci.*, **180**, 81 (2001).
31. P. M. Mooney, *J. Appl. Phys.*, **67**, R1 (1990).
32. J. Uzuhashi and T. Ohkubo, *Ultramicroscopy*, **262**, 113980 (2024).
33. J. Uzuhashi, Y. Yao, T. Ohkubo, and T. Sekiguchi, *Microscopy*, **74**, 279 (2025).
34. J. P. Perdew, A. Ruzsinszky, G. I. Csonka, O. A. Vydrov, G. E. Scuseria, L. A. Constantin, X. Zhou, and K. Burke, *Phys. Rev. Lett.*, **100**, 136406 (2008).
35. T. Yamasaki, A. Kuroda, T. Kato, J. Nara, J. Koga, T. Uda, K. Minami, and T. Ohno, *Comput. Phys. Commun.*, **244**, 264 (2019).
36. J. Uzuhashi, Y. Irokawa, T. Nabatame, Y. Koide, and T. Ohkubo, *AIP Adv.*, **16**, 045004 (2026).
37. D. S. Sholl and J. A. Steckel, *Density Functional Theory* (Wiley, New Jersey) 179 (2009).
38. V. Darakchieva, B. Monemar, and A. Usui, *Appl. Phys. Lett.*, **91**, 031911 (2007).
39. W. M. Chen, I. A. Buyanova, M. Wagner, B. Monemar, J. L. Lindström, H. Amano, and I. Akasaki, *MRS Internet J. Nitride Semicond. Res.*, **4**, 514 (1999).
40. R. Y. Korotkov and B. W. Wessels, *MRS Internet J. Nitride Semicond. Res.*, **5**, 301 (2000).
41. M. N. R. Ashfold, J. P. Goss, B. L. Green, P. W. May, M. E. Newton, and C. V. Peaker, *Chem. Rev.*, **120**, 5745 (2020).
42. D. J. Chadi and K. J. Chang, *Phys. Rev. B*, **39**, 10063 (1989).
43. T. N. Theis, P. M. Mooney, and S. L. Wright, *Phys. Rev. Lett.*, **60**, 361 (1988).
44. M. Kočan, A. Rizzi, H. Lüth, S. Keller, and U. K. Mishra, *Phys. Stat. Sol. (b)*, **234**, 773 (2002).
45. Y. Dong, R. M. Feenstra, and J. E. Northrup, *J. Vac. Sci. Technol. B*, **24**, 2080 (2006).
46. D. Majchrzak, M. Grodzicki, P. Ciechanowicz, J. G. Rousset, E. Piskorska-Hommel, and D. Hommel, *Acta Phys. Pol. A.*, **136**, 285 (2019).